Offset simultaneous conjugate atom interferometers

Weicheng Zhong,[*] Richard H. Parker, Zachary Pagel, Chenghui Yu,[†] and Holger Müller[‡]
Department of Physics, University of California, Berkeley, California 94720, USA

(Received 11 January 2019; revised manuscript received 15 April 2020; accepted 16 April 2020; published 14 May 2020)

Correlating the signals from simultaneous atom interferometers has enabled some of the most precise determinations of fundamental constants. Here, we show that multiple simultaneous interferometers with strategically chosen initial conditions (offset simultaneous conjugate interferometers) can provide multichannel readouts that measure or suppress specific signals and systematic effects. We create two pairs of simultaneous conjugate interferometers and precisely control the offset between them with Bragg diffraction and Bloch oscillations. This allows us to cancel the effect of acceleration gradients, a major systematic effect in many atom interferometry measurements. It also reduces the undesired diffraction phase from Bragg diffraction beam splitters by a factor of 6. This work paves the way for measurements of the fine-structure constant below the 10-part-per-trillion level. It can also be generalized for isotope-mass-ratio measurements.

DOI: 10.1103/PhysRevA.101.053622

I. INTRODUCTION

Atom interferometers have been used for inertial sensing [1–5], testing Einstein's equivalence principle [6–10], measuring Newton's gravitational constant G [11,12], and searching for dark-sector particles [13,14]. Running two interferometers simultaneously and interrogating them with the same laser (simultaneous conjugate atom interferometers, or SCIs) has proven to cancel several systematic effects and has led to the most accurate determination of the fine-structure constant α [15]. Many common-mode effects, such as vibrations and uniform gravitational acceleration, are suppressed in the differential phase between these two interferometers. Gravity gradients and diffraction phases [16,17], however, which can be thousands of times as large as needed for the final accuracy, remain.

we propose and demonstrate a scheme: offset simultaneous conjugate interferometers (OSCIs; Fig. 1), which can exactly cancel the effects of acceleration gradients (due to, for example, a gravity gradient, inhomogeneous magnetic fields [15], blackbody radiation [18], etc.) and substantially reduce diffraction phases from Bragg diffraction beam splitters [19,20]. We split one atom sample into two using one Bragg diffraction pulse and two Bloch oscillation sequences [21], creating two sets of SCIs to form a multichannel interferometer. The vertical offset between the two SCIs is precisely controlled by the timing of these two Bloch oscillation sequences. Different channels of this geometry can be used to amplify or suppress specific signals. Importantly, the offset required to cancel the gradient is independent of the magnitude of the gradient. We also demonstrate that the undesired diffraction phase [20] from the Bragg beam splitters is suppressed due to the symmetry of this geometry. Finally, we discuss the potential for using OSCIs to measure the fine-structure constant α.

II. CANCELING THE ACCELERATION GRADIENT PHASE

For an atom interferometer where the atomic wave packets travel along the lower arm z_l and upper arm z_u, a vertical acceleration gradient γ will introduce a phase shift, to first order in γ, as

$$\phi_\gamma = \frac{m\gamma}{2\hbar}\int (z_l^2 - z_u^2)dt = \frac{m\gamma A z_c}{\hbar}, \tag{1}$$

where m is the mass of the atom, $\hbar$ is the reduced Planck constant, $A = \int (z_l - z_u)dt$ is the space-time area enclosed between the two arms, and $z_c = \int (z_l^2 - z_u^2)dt/2A$ is the center of this space-time area.

For two simultaneous interferometers whose centers are separated by a vertical distance δz, the differential phase shift caused by γ is

$$\delta\phi_\gamma = \frac{m\gamma A}{\hbar}\delta z. \tag{2}$$

This γ-related phase is an important systematic error source in many atom interferometer applications [12,15,22,23]. Several schemes have been proposed to control this effect [24–27]. However, so far these schemes require the gravity gradient to be measured, necessarily introducing a corresponding uncertainty. They also involve changing the frequency of the laser beams, which will complicate other systematic effects, such as diffraction phases. OSCIs cancel the effect from acceleration gradients by overlapping the centers of the two simultaneous interferometers, so that $\delta z = 0$ and $\delta\phi_\gamma$ vanishes according to Eq. (2). Not only does this technique not require

[*]zhongw@berkeley.edu
[†]Present address: Department of Physics, University of California, San Diego, 9500 Gilman Drive, La Jolla, California 92093, USA.
[‡]Also at Molecular Biophysics and Integrated Bioimaging, Lawrence Berkeley National Laboratory, One Cyclotron Road, Berkeley, California 94720, USA.

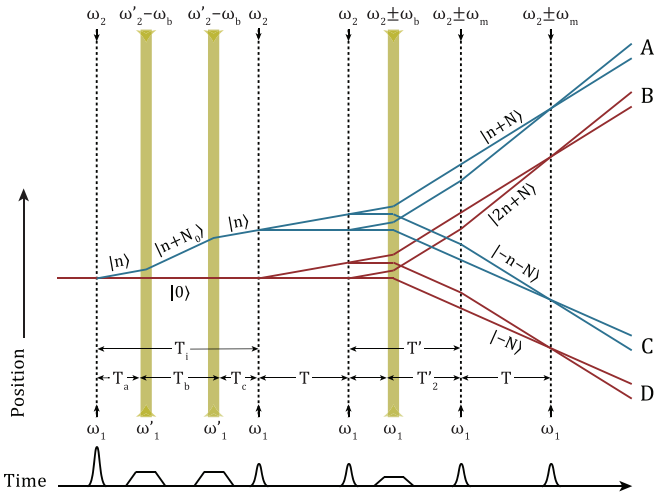

FIG. 1. The top panel shows the pulse sequence and atom trajectories in OSCIs. Every dashed line represents a pair of counter-propagating laser pulses that drive Bragg diffraction. Bands represent the optical lattices that drive Bloch oscillations. We split the atom sample into two with one Bragg pulse and two Bloch oscillation sequences and create two sets of SCIs (the blue one and the red one). The four output ports A to D constitute four output channels. Among these four channels, AC and BD are similar to the SCIs used previously, BC is the γ-insensitive channel, and AD is the channel most sensitive to γ. Momentum states are indicated above the lines. In the bottom are the temporal profiles of all the laser pulses. Bragg pulses have Gaussian temporal profiles. Bloch oscillations have trapezoid temporal profiles.

a measurement of γ, it also works for both Bragg and Raman beam splitters and can be applied to any atom interferometer geometry, even the ones that are not intended for a gravity measurement, like Ramsey-Bordé interferometers.

Figure 1 shows the geometry of OSCIs. We first apply an nth-order Bragg pulse, which transfers the momentum of $2n$ photons and drives the atoms into a superposition of states $|0\rangle$ and $|n\rangle$ ($|n\rangle$ denotes a momentum eigenstate with a momentum of $2n$ photons). After time T_a, Bloch oscillations are applied to accelerate the upper arm to the state $|n+N_0\rangle$. A second deceleration Bloch oscillation sequence then brings this arm back to state $|n\rangle$. As the relative motion of these two arms comes from photon recoils, the displacement between them can be precisely controlled by the timing of these two Bloch oscillation beams. The initial Bragg pulse and the two Bloch oscillation sequences do not participate in interference. They are referred to as the offset-generating Bragg and Bloch beams later in this paper. After another interval T_c, we apply a pair of nth-order Bragg beam splitters, a sequence of N Bloch oscillations, and another pair of nth-order Bragg beam splitters. Each pair of Bragg beam splitters has a separation time of T, and the two pairs are separated by time T'. The second pair of Bragg beam splitters contains two frequencies, which are shifted by $\pm\omega_m$ relative to the first pair. These beams are referred to as interferometer Bragg and Bloch beams. In the end, we have two sets of SCIs (the blue one and the red one) and four output ports (A to D), which constitute four output channels. Among these four channels, AC (a channel that outputs the differential phase between A and C) and BD are similar to the SCIs used previously. BC is the γ-insensitive channel, as B and C are spatially overlapped and can be used to cancel the γ effect. AD, AC, and BD are sensitive to γ, with AD having the largest sensitivity because it has the largest displacement.

III. DERIVATION OF THE REQUIRED OFFSET

The offset-generating beams will offset the two SCIs by

$$\delta z = 2v_r(nT_i + N_0T_b), \tag{3}$$

where $v_r = \hbar k/m_{Cs}$ is the recoil velocity of a cesium atom with mass m_{Cs} after scattering a photon with wave number k. Using Eq. (2), this offset will cause a phase shift

$$\delta\phi_\gamma = 8nT\omega_r\gamma(T + T')(nT_i + N_0T_b), \tag{4}$$

where $\omega_r = mv_r^2/(2\hbar)$ is the recoil frequency. T_i, T_b, T, and T' are pulse-separation times defined in Fig. 1. This phase shift has opposite signs on channel AD and BC.

The overall differential phase Φ from channel AC (or BD) was derived in Ref. [15]. Including the offset phase shift, the differential phase from every channel IJ ($IJ \in \{AC, BD, BC, AD\}$) now can be summarized as

$$\Phi = -2nT[\omega_m - 8\omega_r(n + N) - \omega_r\gamma C_{IJ}] + \phi_{IJ}, \tag{5}$$

where ϕ_{IJ} is the overall diffraction phase on every channel; C_{IJ} is the channel-dependent coefficient of the γ-related phase:

$$\begin{aligned} C_{BD} &= \frac{2}{3}n(2T^2 + 3TT' + 3T'^2) \\ &\quad + \frac{4}{3}N(T^2 + 3TT_2' + 3T_2'^2), \\ C_{AC} &= C_{BD}, \\ C_{AD} &= C_{BD} + 4(nT_i + N_0T_b)(T + T'), \\ C_{BC} &= C_{BD} - 4(nT_i + N_0T_b)(T + T'). \end{aligned} \tag{6}$$

High-order effects, including the phase terms that depend on the atom velocity, the duration of the Bloch beam, and the gravity acceleration g, are not shown for simplicity [15]. By properly tuning the timing of the second offset-generating Bloch beam, we can cancel C_{BC}, thus suppressing the γ effect on channel BC. In the meantime, C_{AD} will be doubled, and channel AD will have higher sensitivity to γ compared to AC and BD.

IV. SUPPRESSING THE DIFFRACTION PHASE

Bragg diffraction is a key technique used in many atom interferometer applications [16,17,28]. Compared to conventional two-photon Raman transitions, Bragg diffraction transfers multiple photon momenta every time, which increases the space-time area enclosed between the different arms of the interferometer, thus improving the sensitivity. As atoms remain in the same internal electronic state, important systematic effects, like the Zeeman and Stark effects, are suppressed. But Bragg diffraction coherently couples atoms to unwanted momentum states and inevitably causes undesired diffraction phase. This diffraction phase depends on the duration, intensity, and shape of the laser pulses, on the Bragg diffraction order, and on the detuning from two-photon resonance. It

is hard to control in experiments or calculate analytically. Therefore, the diffraction phase represents a major source of systematic uncertainty in precision measurements [19,20].

The diffraction phase is suppressed in the γ-insensitive channel BC, which can be seen by examining the symmetries of OSCIs. After the offset-generating Bragg and Bloch beams, the upper SCI (the blue one) starts from the state $|n\rangle$, and the lower SCI (the red one) starts from the state $|0\rangle$. The two interferometers of channel BC now have a symmetric configuration compared to the regular SCI channel BD (or AC) where the two interferometers start from the same momentum state. This symmetry leads to the cancellation of the diffraction phase from the first two interferometer Bragg pulses. To show that, we follow the analysis in Refs. [19,20]. We use $\hat{B}_n$ to denote an nth-order Bragg pulse. By numerically solving the optical Bloch equations that describe the process of Bragg diffraction [20], we obtain the matrix element $\langle b|\hat{B}_n|a\rangle$ as the complex amplitude for the Bragg pulse to drive an atom from state $|a\rangle$ into state $|b\rangle$. The diffraction phase from the beam splitter $\hat{B}_n$ is thus the argument $\arg(\langle b|\hat{B}_n|a\rangle)$,

Denote the diffraction phase from the mth interferometer Bragg pulse on output port I ($I \in \{A, B, C, D\}$) as $\phi_{I,m}$. For A, the first interferometer Bragg pulse does not change the upper arm's state $|n\rangle$ but drives the lower arm from $|n\rangle$ to $|0\rangle$; thus, $\phi_{A,1} = \arg(\langle n|\hat{B}_n|n\rangle/\langle n|\hat{B}_n|0\rangle)$. Similarly,

$$\phi_{A,1} = \phi_{A,2} = \phi_{B,2} = \phi_{C,1} = \arg\left(\frac{\langle n|\hat{B}_n|n\rangle}{\langle n|\hat{B}_n|0\rangle}\right),$$
$$\phi_{B,1} = \phi_{C,2} = \phi_{D,1} = \phi_{D,2} = \arg\left(\frac{\langle n|\hat{B}_n|0\rangle}{\langle 0|\hat{B}_n|0\rangle}\right). \quad (7)$$

For every channel IJ, the diffraction phase from the mth interferometer Bragg pulse, denoted as $\phi_{IJ,m}$, is $\phi_{I,m} - \phi_{J,m}$. Using Eq. (7),

$$\phi_{AC,1} = \phi_{BD,1} = 0,$$
$$\phi_{AD,1} = -\phi_{BC,1} = \phi_{AC,2} = \phi_{BD,2} = \phi_{AD,2}$$
$$= \phi_{BC,2} = \arg\left(\frac{\langle 0|\hat{B}_n|0\rangle\langle n|\hat{B}_n|n\rangle}{\langle n|\hat{B}_n|0\rangle^2}\right). \quad (8)$$

Because $\phi_{AC,1} = \phi_{BD,1} = 0$, the diffraction phase from the first two Bragg pulses is zero in channels AC and BD, and the main contribution comes from the second one. In the γ-insensitive channel BC, the diffraction phases from the first two interferometer Bragg pulses cancel each other because $\phi_{BC,1} = -\phi_{BC,2} = 0$; conversely, in channel AD, the first two interferometer Bragg pulses introduce the same diffraction phase. A similar analysis shows that the diffraction phase from the third and fourth interferometer Bragg pulses is the same in all channels. Therefore, the overall diffraction phase is suppressed in channel BC and amplified in channel AD relative to channels AC and BD.

V. EXPERIMENT

Our setup is similar to the one in Ref. [19]. Cesium atoms are first loaded into a magneto-optical trap and launched upward via moving optical molasses [29]. The atoms are then further cooled to a few hundred nanokelvins with Raman sideband cooling [30]. With three subsequent Raman transitions, we prepare cesium atoms into the $|F = 3, m_F = 0\rangle$ electronic state with a velocity spread less than 0.1 recoil velocities along the vertical direction. Bragg and Bloch beams are then applied during the flight, as shown in Fig. 1. When the atoms fall back down, we apply a resonant detection beam and detect the fluorescences. The whole sequence is repeated every 2.4 s.

We use fifth-order Bragg pulses ($n = 5$) and 125 Bloch oscillations ($N_0 = N = 125$) for offset generation and the interferometer. All the Bragg and Bloch beams are 15 GHz blue detuned from the cesium $|F = 3\rangle \rightarrow |F' = 4\rangle$ D_2 transition. The intensity of the offset-generating Bragg pulse is set so that output ports A and B have roughly the same signal amplitude. The intensities of the two offset-generating Bloch oscillation beams are optimized to the highest efficiency. The frequencies of the offset-generating Bloch beams are generated in the same way as the interferometer Bloch beams. So the down-propagating beams contain a pair of frequencies. For them to interact with the atoms in the momentum state $|n\rangle$, the frequencies of the counterpropagating beams are decreased by 20 kHz: $\omega_2 - \omega_2' = \omega_1 - \omega_1' = 2\pi \times 20$ kHz. Atoms left behind by the acceleration Bloch oscillations are mostly in the $|n\rangle$ state and would spatially overlap with the signals. To suppress these atoms, we apply a velocity-sensitive two-photon Raman pulse to drive the atoms with $2n\hbar k$ momentum from the $|F = 3\rangle$ ground state to the $|F = 4\rangle$ ground state and then apply a resonant beam to blow away the atoms in the $|F = 4\rangle$ state. These pulses are not shown in Fig. 1. Atoms left behind by the deceleration Bloch oscillations are in the $|n + N_0\rangle$ momentum state. They are spatially resolved from the output channels and thus will not affect the experiment.

We fix the timing of the offset-generating Bragg pulse, the acceleration offset-generating Bloch oscillations, and the second and the third interferometer Bragg pulses relative to the experiment sequence: $T_a = 5$ ms, $T_i + T = 155$ ms, $T' = 50$ ms, and $T_2' = 45$ ms. When T changes, we adjust T_b according to Eq. (6), so that $C_{BC} = 0$. This guarantees channel BC has no sensitivity to γ.

A. Statistical sensitivity

First, we demonstrate the statistical sensitivity of OSCIs. We set T to 10 ms. T_b is calculated to be 37.6 ms from Eq. (6). This results in an offset of about 3.2 cm between the two wave packets at the moment of the first interferometer Bragg pulse. Figure 2(a) shows the typical fluorescence signal we observe. The eight peaks on the two sides correspond to four output ports. The two peaks in the middle come from the atoms that are not driven by the interferometer Bloch oscillations. These atoms do not contribute to the measurement.

We use ellipse fitting [31,32] to extract the differential phase between two output ports. The ellipses are shown in Fig. 2(b). The x axis of each ellipse is the normalized signal of the lower interferometer (C or D), and the y axis is the normalized signal of the upper interferometer (A or B). The γ-insensitive channel BC has the same x contrast as channel AC (about 16%) and the same y contrast as channel BD (about 22%), demonstrating that introducing an offset does not lead to decoherence. After 13 h of integration, we reach an uncertainty of about 3 parts per billion (ppb) in the differential phase for every channel, which corresponds to

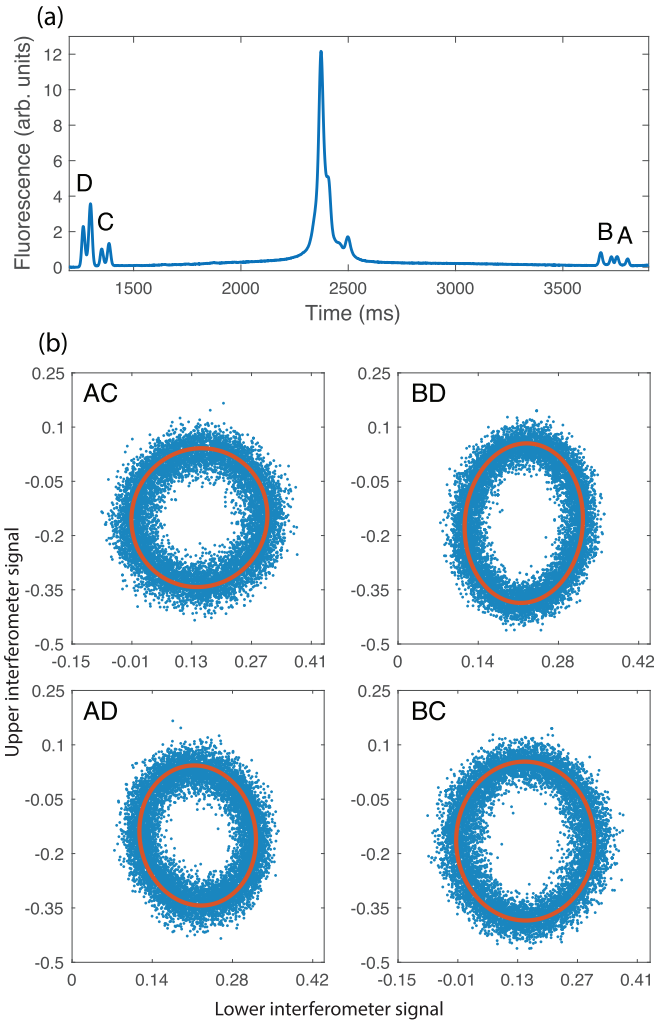

FIG. 2. (a) Fluorescence trace taken at $T = 10$ ms and $T_b = 37.6$ ms. It is an average of 30 measurements. The eight peaks on the two sides correspond to four output ports. The two big peaks in the middle are the atoms not driven by Bloch oscillations, which do not contribute to the measurement. (b) Signal from every channel. The x axis is the normalized signal of the lower interferometers (C or D), and the y axis is the normalized signal of the upper interferometers (A or B). Data were collected over a period of 13 h. The red curve is the fitted ellipse from every channel.

1.5 ppb statistical uncertainty in α [15]. This demonstrates the world-class sensitivity of OSCIs.

Figure 3 shows the Allan deviation of the measured frequency for every OSCI channel. The sensitivities of all channels are about the same, roughly at $1.1\,\mathrm{Hz}/\sqrt{\mathrm{Hz}}$. As a comparison, we remove the offset-generating beams and leave the interferometer beam sequence unchanged. This leads to a regular SCI geometry. The Allan deviation for this SCI geometry is also plotted, showing a sensitivity of $0.38\,\mathrm{Hz}/\sqrt{\mathrm{Hz}}$. The sensitivity of every OSCI channel is reduced by only a factor of 3 compared to the SCI geometry. This reduction can be explained by two aspects. First, OSCIs distribute the atom population on four output ports. This reduces the effective signal size on each channel. Second, single-photon scattering introduced by the two offset-generating Bloch oscillation

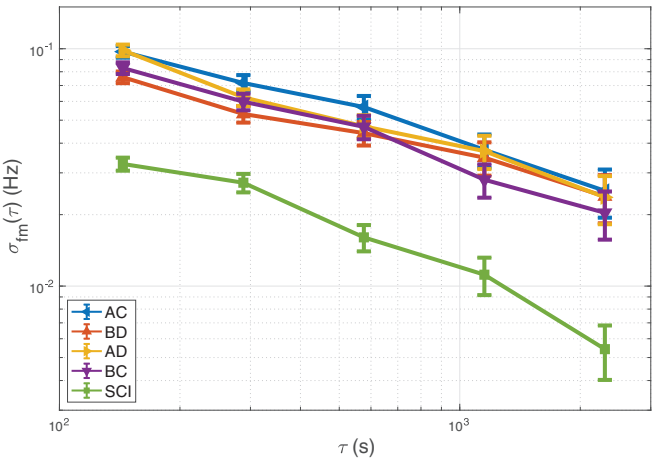

FIG. 3. Allan deviation of the measured frequency at $T = 10$ ms for every OSCI channel. As a comparison, the Allan deviation for the SCI geometry with the same interferometer timing sequence is also plotted.

sequences further lowers the total signal size. Increasing the detuning of the laser pulses to suppress single-photon scattering and using broader laser beams to drive Bragg diffraction and Bloch oscillations (so the intensity is more uniform across the atomic sample) are expected to improve the signal-to-noise ratio, thus benefitting the sensitivity.

B. Consistent output and suppression of the diffraction phase

Next, we show the consistency of the recoil frequency from every channel and the suppression of the diffraction phase. We vary the pulse separation time T from 5 to 20 ms and adjust T_b accordingly. At each T, we adjust ω_m to the point where the total phase Φ is zero. Define the measured frequency as $f_m = \omega_m/(2\pi)$. According to Eqs. (5) and (6), f_m can be fitted as a function of $1/T$ with two fitting parameters, the diffraction phase and the recoil frequency $f_r = \omega_r/(2\pi)$,

$$f_m = \frac{\phi_{IJ}}{4n\pi T} + [8(n+N) + \gamma \times C_{IJ}]f_r. \tag{9}$$

Figure 4(a) shows the measurement results and the corresponding fittings. At short T's, the contribution from the gravity gradient is small. f_m is roughly linear in $1/T$, with a slope proportional to the diffraction phase. The coefficients C_{IJ} scale with T^2. As T increases, the effect from the gravity gradient becomes more pronounced; thus, the fitting curve is no longer linear. This represents a potentially large systemic effect in the α measurement. For instance, at $T = 80$ ms, the gravity gradient will shift the total phase in channel BD by 8 ppb, which is over two orders of magnitude larger than the required accuracy of the recoil frequency. By properly setting the timing, sensitivity to γ in channel BC is canceled. The fitting for this channel is a straight line.

Figure 4(b) shows the fitted recoil frequencies from all channels. They agree with each other within 1σ uncertainty, demonstrating the consistency of the output from every channel. Figure 4(c) shows the fitted diffraction phase from all channels: $\phi_{AC} = 22 \pm 6$ mrad, $\phi_{BD} = 41 \pm 3$ mrad,

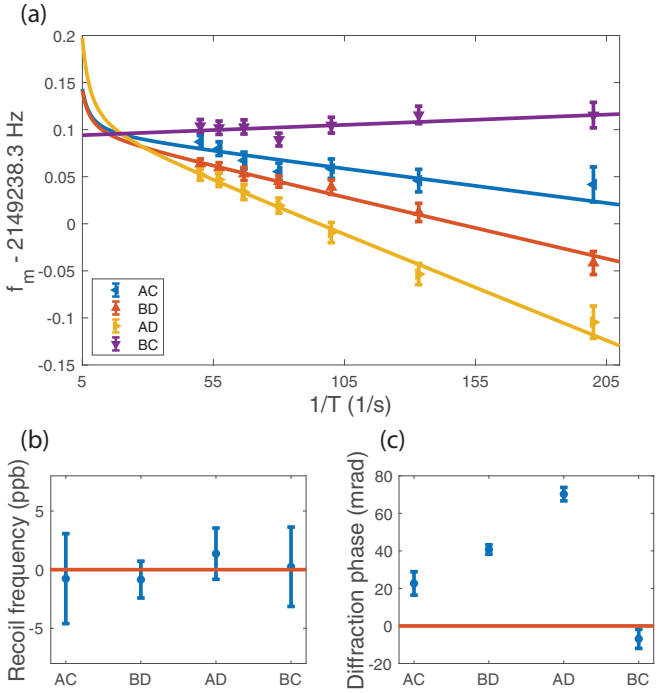

FIG. 4. (a) Measured frequency vs $1/T$. The data points are from experimental measurements, and curves are corresponding fittings using the functional form of Eq. (9). The γ value comes from Ref. [15]. Channel *BC* has no γ effect; the fitting is a straight line. Data were taken over two successive days. (b) Fitted recoil frequencies in all channels. They are consistent within in 1σ uncertainty. The red line is the average of these frequencies. (c) Fitted diffraction phases from all channels. The red line indicates zero. A sixfold suppression of the diffraction phase in channel *BC* was observed compared to channel *BD*.

$\phi_{AD} = 70 \pm 4\,\text{mrad}$, and $\phi_{BC} = -7 \pm 5\,\text{mrad}$. The diffraction phase is suppressed by a factor of 6 in channel *BC* compared to channel *BD* and a factor of 10 compared to channel *AD*.

VI. DISCUSSION AND CONCLUSIONS

A measurement of α using atom interferometers has two leading systematic error sources: acceleration gradients and non-Gaussian wave fronts [15]. With this OSCI scheme, the uncertainty from the acceleration gradient will now be negligible. The effects from non-Gaussian wave fronts can be suppressed by driving Bragg diffraction and Bloch oscillations with larger-width laser beams, which, as mentioned above, also improves the sensitivity. Combining with other upgrades described in [33], we expect to improve the accuracy of α to the 10-part-per-trillion level, which would provide a test of the standard model improved by a factor of 20 when paired with similar improvement in the electron $g_e - 2$ measurement [34].

The ability to control the offset in OSCIs also enables new ways to check many systematic effects. For example, with the increased vertical separation between *A* and *D*, OSCIs can measure γ using channel *AD*. Comparing the results from channels *AC* and *BD* allows us to identify and reduce effects such as the inhomogeneous magnetic field along the vertical direction, the divergence of the laser beams, and the stray light reflected by the vacuum chamber [15]. Because these two channels have the same phase produced by the gravity gradient, a comparison between them will also place a bound on third-order gravity variation (the gradient of the gravity gradient). These systematic checks can be done simultaneously with data taken for a measurement of the recoil frequency.

The OSCI geometry can also be generalized for isotope-mass-ratio measurements [35]. With sensitivity to the mass of atoms and immunity to gravity gradients, OSCIs provides a compelling scheme for precision mass-ratio measurements with matter-wave interferometers.

ACKNOWLEDGMENTS

This work is supported by the Jet Propulsion Laboratory (Grant No. 1612859), the National Institute of Standards and Technology (Grant No. 60NANB17D311), the National Science Foundation (Grant No. 1806583), and the William M. Keck Foundation (Grant No. 042982). This work was also partially supported by the Office of Science, Office of High Energy Physics, of the US Department of Energy, under Contract No. DE-AC02-05CH11231. In particular, support comes from the Quantum Information Science Enabled Discovery (QuantISED) program for High Energy Physics (KA2401032).

[1] A. Peters, K. Y. Chung, and S. Chu, Measurement of gravitational acceleration by dropping atoms, Nature (London) **400**, 849 (1999).

[2] R. Geiger, V. Ménoret, G. Stern, N. Zahzam, P. Cheinet, B. Battelier, A. Villing, F. Moron, M. Lours, Y. Bidel, A. Bresson, A. Landragin, and P. Bouyer, Detecting inertial effects with airborne matter-wave interferometry, Nat. Commun. **2**, 474 (2011).

[3] A. Sugarbaker, S. M. Dickerson, J. M. Hogan, D. M. S. Johnson, and M. A. Kasevich, Enhanced Atom Interferometer Readout through the Application of Phase Shear, Phys. Rev. Lett. **111**, 113002 (2013).

[4] I. Dutta, D. Savoie, B. Fang, B. Venon, C. L. Garrido Alzar, R. Geiger, and A. Landragin, Continuous Cold-Atom Inertial Sensor with 1 nrad/sec Rotation Stability, Phys. Rev. Lett. **116**, 183003 (2016).

[5] M. Xin, W. S. Leong, Z. Chen, and S.-Y. Lan, An atom interferometer inside a hollow-core photonic crystal fiber, Sci. Adv. **4**, e1701723 (2018).

[6] S. Fray, C. A. Diez, T. W. Hänsch, and M. Weitz, Atomic Interferometer with Amplitude Gratings of Light and Its Applications to Atom Based Tests of the Equivalence Principle, Phys. Rev. Lett. **93**, 240404 (2004).

[7] D. Schlippert, J. Hartwig, H. Albers, L. L. Richardson, C. Schubert, A. Roura, W. P. Schleich, W. Ertmer, and E. M. Rasel, Quantum Test of the Universality of Free Fall, Phys. Rev. Lett. **112**, 203002 (2014).

[8] M. G. Tarallo, T. Mazzoni, N. Poli, D. V. Sutyrin, X. Zhang, and G. M. Tino, Test of Einstein Equivalence Principle for 0-Spin and Half-Integer-Spin Atoms: Search for Spin-Gravity Coupling Effects, Phys. Rev. Lett. **113**, 023005 (2014).

[9] L. Zhou, S. Long, B. Tang, X. Chen, F. Gao, W. Peng, W. Duan, J. Zhong, Z. Xiong, J. Wang, Y. Zhang, and M. Zhan, Test of Equivalence Principle at 10^{-8} Level by a Dual-Species Double-Diffraction Raman Atom Interferometer, Phys. Rev. Lett. **115**, 013004 (2015).

[10] X.-C. Duan, X.-B. Deng, M.-K. Zhou, K. Zhang, W.-J. Xu, F. Xiong, Y.-Y. Xu, C.-G. Shao, J. Luo, and Z.-K. Hu, Test of the Universality of Free Fall with Atoms in Different Spin Orientations, Phys. Rev. Lett. **117**, 023001 (2016).

[11] J. B. Fixler, G. T. Foster, J. M. McGuirk, and M. A. Kasevich, Atom interferometer measurement of the newtonian constant of gravity, Science **315**, 74 (2007).

[12] G. Rosi, F. Sorrentino, L. Cacciapuoti, M. Prevedelli, and G. M. Tino, Precision measurement of the Newtonian gravitational constant using cold atoms, Nature (London) **510**, 518 (2014).

[13] B. Elder, J. Khoury, P. Haslinger, M. Jaffe, H. Müller, and P. Hamilton, Chameleon dark energy and atom interferometry, Phys. Rev. D **94**, 044051 (2016).

[14] P. Hamilton, M. Jaffe, P. Haslinger, Q. Simmons, H. Müller, and J. Khoury, Atom-interferometry constraints on dark energy, Science **349**, 849 (2015).

[15] R. H. Parker, C. Yu, W. Zhong, B. Estey, and H. Müller, Measurement of the fine-structure constant as a test of the standard model, Science **360**, 191 (2018).

[16] S.-w. Chiow, T. Kovachy, H.-C. Chien, and M. A. Kasevich, $102\hbar k$ Large Area Atom Interferometers, Phys. Rev. Lett. **107**, 130403 (2011).

[17] H. Müller, S.-w. Chiow, and S. Chu, Atom-wave diffraction between the Raman-Nath and the Bragg regime: Effective Rabi frequency, losses, and phase shifts, Phys. Rev. A **77**, 023609 (2008).

[18] P. Haslinger, M. Jaffe, V. Xu, O. Schwartz, M. Sonnleitner, M. Ritsch-Marte, H. Ritsch, and H. Müller, Attractive force on atoms due to blackbody radiation, Nat. Phys. **14**, 257 (2018).

[19] B. Estey, C. Yu, H. Müller, P.-C. Kuan, and S.-Y. Lan, High-Resolution Atom Interferometers with Suppressed Diffraction Phases, Phys. Rev. Lett. **115**, 083002 (2015).

[20] R. H. Parker, C. Yu, B. Estey, W. Zhong, E. Huang, and H. Müller, Controlling the multiport nature of Bragg diffraction in atom interferometry, Phys. Rev. A **94**, 053618 (2016).

[21] R. Bouchendira, P. Cladé, S. Guellati-Khélifa, F. Nez, and F. Biraben, New Determination of the Fine Structure Constant and Test of the Quantum Electrodynamics, Phys. Rev. Lett. **106**, 080801 (2011).

[22] A. M. Nobili, Fundamental limitations to high-precision tests of the universality of free fall by dropping atoms, Phys. Rev. A **93**, 023617 (2016).

[23] J. Williams, S.-w. Chiow, N. Yu, and H. Müller, Quantum test of the equivalence principle and space-time aboard the international space station, New J. Phys. **18**, 025018 (2016).

[24] S.-w. Chiow, J. Williams, N. Yu, and H. Müller, Gravity-gradient suppression in spaceborne atomic tests of the equivalence principle, Phys. Rev. A **95**, 021603(R) (2017).

[25] A. Roura, Circumventing Heisenberg's Uncertainty Principle in Atom Interferometry Tests of the Equivalence Principle, Phys. Rev. Lett. **118**, 160401 (2017).

[26] G. D'Amico, G. Rosi, S. Zhan, L. Cacciapuoti, M. Fattori, and G. M. Tino, Canceling the Gravity Gradient Phase Shift in Atom Interferometry, Phys. Rev. Lett. **119**, 253201 (2017).

[27] C. Overstreet, P. Asenbaum, T. Kovachy, R. Notermans, J. M. Hogan, and M. A. Kasevich, Effective Inertial Frame in an Atom Interferometric Test of the Equivalence Principle, Phys. Rev. Lett. **120**, 183604 (2018).

[28] B. Plotkin-Swing, D. Gochnauer, K. E. McAlpine, E. S. Cooper, A. O. Jamison, and S. Gupta, Three-Path Atom Interferometry with Large Momentum Separation, Phys. Rev. Lett. **121**, 133201 (2018).

[29] E. L. Raab, M. Prentiss, A. Cable, S. Chu, and D. E. Pritchard, Trapping of Neutral Sodium Atoms with Radiation Pressure, Phys. Rev. Lett. **59**, 2631 (1987).

[30] V. Vuletić, C. Chin, A. J. Kerman, and S. Chu, Degenerate Raman Sideband Cooling of Trapped Cesium Atoms at Very High Atomic Densities, Phys. Rev. Lett. **81**, 5768 (1998).

[31] A. Fitzgibbon, M. Pilu, and R. B. Fisher, Direct least square fitting of ellipses, IEEE Trans. Pattern Anal. Mach. Intell. **21**, 476 (1999).

[32] G. T. Foster, J. B. Fixler, J. M. McGuirk, and M. A. Kasevich, Method of phase extraction between coupled atom interferometers using ellipse-specific fitting, Opt. Lett. **27**, 951 (2002).

[33] C. Yu, W. Zhong, B. Estey, J. Kwan, R. H. Parker, and H. Müller, Atom-interferometry measurement of the fine structure constant, Ann. Phys. (Berlin) **531**, 1800346 (2019).

[34] G. Gabrielse, S. E. Fayer, X. Myers, and T. G. Fan, Towards an improved test of the standard model's most precise prediction, Atoms **7**, 45 (2019).

[35] T. Kovachy, J. M. Hogan, D. M. S. Johnson, and M. A. Kasevich, Optical lattices as waveguides and beam splitters for atom interferometry: An analytical treatment and proposal of applications, Phys. Rev. A **82**, 013638 (2010).